

3D Particle Positions from Computer Stereo Vision in PK-4

Daniel P. Mohr, Peter Huber, Mierk Schwabe, Christina A. Knapek

January 3, 2022

Contents

1	Introduction	1
2	Modeling	2
2.1	Possible Accuracy in View Direction	3
3	Finding Corresponding Features	4
4	Projection to Laser	5
4.1	Projection to Laser Plane	5
4.2	Projection to Laser Sheet	6
5	Conclusion	9
	References	11

1 Introduction

Complex plasmas consist of microparticles embedded in a low-temperature plasma containing ions, electrons and neutral particles. The microparticles form a dynamical system that can be used to study a multitude of effects on the level of the constituent particles [Morfill and Ivlev, 2009]. The microparticles are usually illuminated with a sheet of laser light, and the scattered light can be observed with digital cameras — see Figure 1. Mohr *et al.* [2019] describe the feature (particle) detection in a single image/frame. Some complex plasma microgravity research facilities [Pustynnik *et al.*, 2016] use two cameras with an overlapping field of view. Zaehring *et al.* [2018] describes

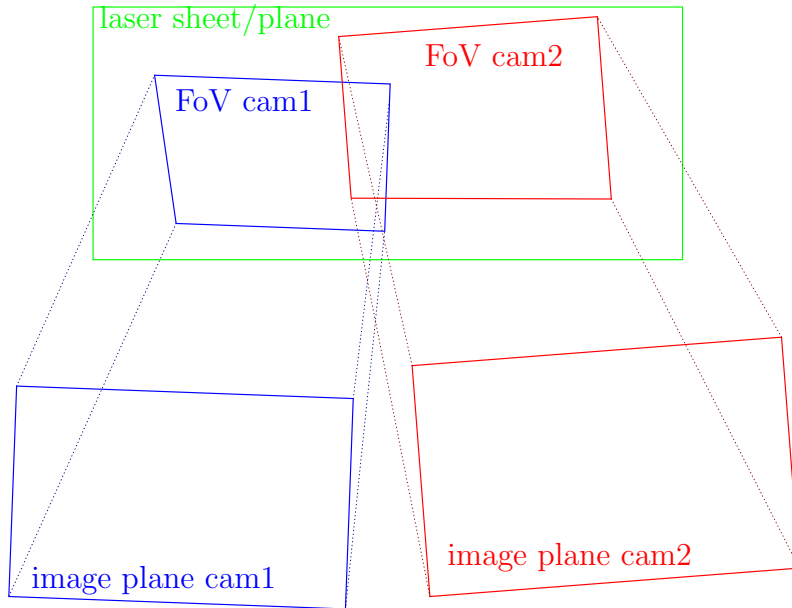


Figure 1: General camera setup of the PK-4 experimental apparatus. This is only a sketch to show the general concept – e. g. scale, angles does not reflect the real situation.

this for a parabolic flight setup of Ekoplasma. Other facilities use even more cameras [Himpel *et al.*, 2011].

An overlapping field of view can be used to combine the resulting images into one and trace the particles in the larger field of view. In previous work this was discussed for the images recorded by the PK-4 Laboratory on board the International Space Station [Schwabe *et al.*, 2019]. In that work the width of the laser sheet was, however, not taken into account. In this paper, we will discuss how to improve the transformation of the features into a joint coordinate system, and possibly extract information on the 3D position of particles in the overlap region.

2 Modeling

In this section the standard model for computer stereo vision Hartley and Zisserman [2004] is briefly touched in a scope necessary for this document. This model is widely used and is, for example, available as an open source implementation Bradski [2000].

The standard model for computer stereo vision uses the pinhole camera model: We can describe the mapping from world coordinates $x \in \mathbb{R}^3$ to image

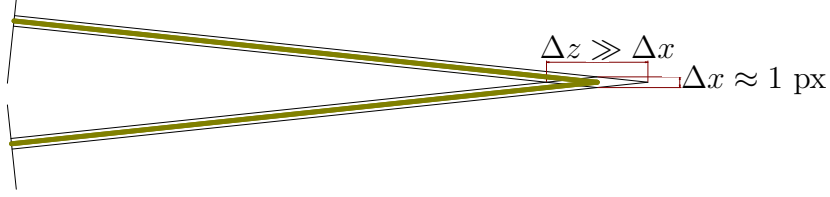


Figure 2: View of two cameras with a small angle of α .

coordinates $p \in \mathbb{R}^2$ up to a scaling parameter s :

$$s \begin{pmatrix} p \\ 1 \end{pmatrix} = \underbrace{C_i (R_i | t_i)}_{=: P_i} \begin{pmatrix} x \\ 1 \end{pmatrix}$$

with

$$\begin{aligned} C_i &\in \mathbb{R}^{3 \times 3} : \text{camera matrix of camera } i \\ R_i &\in \mathbb{R}^{3 \times 3} : \text{rotation matrix of camera } i \\ t_i &\in \mathbb{R}^3 : \text{translation vector of camera } i \\ P_i &\in \mathbb{R}^{3 \times 4} : \text{projection matrix of camera } i. \end{aligned}$$

In addition we use the rational distortion model, which is also used by opencv [Bradski, 2000; Claus and Fitzgibbon, 2005].

2.1 Possible Accuracy in View Direction

If we consider a feature that is represented by a single pixel in each camera — see Figure 2 — we see that the intersection is a parallelogram. The lengths of the diagonals of the parallelogram, Δz and Δx , in relation to the height of the feature, $h = 1$ px, are:

$$\sqrt{\left(\frac{h}{\sin \beta}\right)^2 + \left(\frac{h}{\sin \alpha}\right)^2 \pm 2 \frac{h}{\sin \beta} \frac{h}{\sin \alpha} \cos \alpha},$$

where α is the angle of view and $\beta = \pi - \alpha$.

The PK-4 setup uses the camera Basler Pilot piA1600-35gm [Pustynnik *et al.*, 2016] with a chip of 11.9 mm \times 8.9 mm) and a 50 mm objective lens. The field of view is about 22.4 mm \times 16.8 mm. In the overlap we get:

- $\alpha = 11^\circ$
- $\Delta z \approx 10 \text{ px} \gg 1 \text{ px} \approx \Delta x$

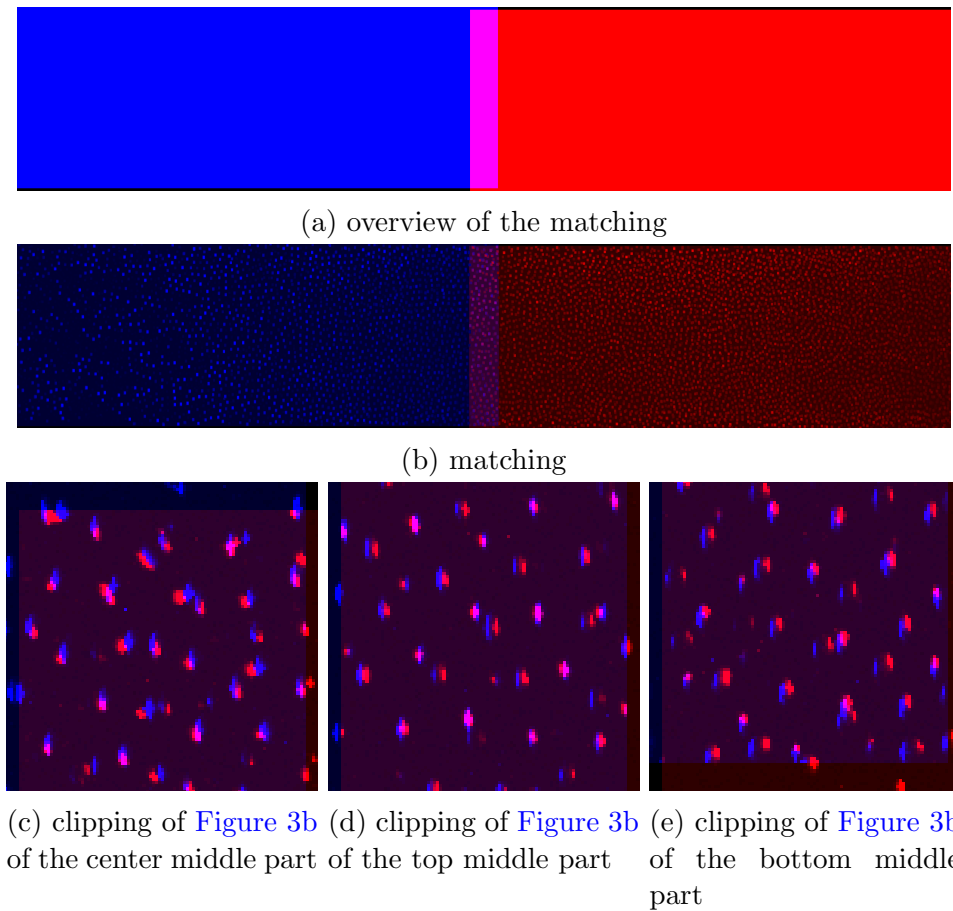


Figure 3: Two images are combined using the common technique template matching. This means only translations are used to embed the right (red) image in the left (blue) one.

3 Finding Corresponding Features

Since the images of the two cameras of the PK-4 setup are very similar in the overlapping region, we can identify corresponding features just by looking at the same position. Therefore we need to combine the images from the cameras.

Using a clipping of one image, we can compare it to any possible clipping of the same size of the other image. The similarity measure "Normalized Cosine Similarity" of the vectors $a \in \mathbb{R}^n$ and $b \in \mathbb{R}^n$ is given by:

$$\frac{1}{2} \left(1 + \frac{a \cdot b}{\|a\|_2 \|b\|_2} \right) \in [0, 1]$$

The clipping with the highest similarity allows to combine the image in a simple way as shown in [Figure 3](#). In this combined image [Figure 3b](#) it is easy to identify corresponding features, which then form the basis for the further analysis.

4 Projection to Laser

Typically in computer stereo vision the images of cameras are used to reconstruct the real scene. In complex plasmas only a small area of the real world is illuminated by a laser. Taken this fact into account allows to reduce the epipolar lines from infinitely long lines to short line segments.

4.1 Projection to Laser Plane

In the intersection of the field of views (F_{oV}) of the cameras, the classical approach of a pinhole camera model leads to

$$s_i \begin{pmatrix} p_j^{(i)} \\ 1 \end{pmatrix} = P_i \begin{pmatrix} x_j \\ 1 \end{pmatrix} \text{ for all } x_j \in F_{oV} \subset \mathbb{R}^3$$

Typically the path of a particle is traced in one image plane. This is only meaningful with the assumption that the laser sheet has no depth.

Here, F_{oV} determines the intersection of the field of views of the cameras. The F_{oV} has to be in the laser plane:

$$\forall x_j \in F_{oV} : l^T x_j = 0.$$

In [[Pustylnik et al., 2016](#); [Zaehring et al., 2018](#)] the projection matrices P_1 and P_2 are not known. We have to identify them from the overlapping fields of view.

Let us assume we have corresponding features $p_i^{(j)}$ by identifying the features in the combined image — [Figure 3](#). Now we can write for all features:

$$\begin{pmatrix} p_j^{(1)} \\ 1 \\ p_j^{(2)} \\ 1 \\ 0 \end{pmatrix} = \begin{pmatrix} \frac{1}{s_1} C_1 \left(\begin{array}{c|c} R_1 & t_1 \end{array} \right) \\ \frac{1}{s_2} C_2 \left(\begin{array}{c|c} R_2 & t_2 \end{array} \right) \\ l^T & 0 \end{pmatrix} \begin{pmatrix} x_j \\ 1 \end{pmatrix} \in \mathbb{R}^7$$

This looks like a linear equation, but in the unknowns $f_x^{(i)}$, $f_y^{(i)}$, $c_x^{(i)}$, $c_y^{(i)}$, α_i , β_i , γ_i , t_i and x_j this is nonlinear due to the trigonometric functions in the

rotation matrices. Furthermore, the distortion model (not formulated here) is not linear.

Without loss of generality we can choose a convenient coordinate system and thus we get for the laser plane:

$$\forall x_j \in F_{oV} : x_j^T \begin{pmatrix} 0 \\ 0 \\ 1 \end{pmatrix} = 0.$$

If we assume to have $n \geq 5$ corresponding pairs of features, this leads to an overdetermined system of equations, and we have to find the best solution:

$$\begin{aligned} \text{obj. func.: } & \sum_{j=1}^n \left\| \begin{pmatrix} p_j^{(1)} \\ 1 \\ p_j^{(2)} \\ 1 \end{pmatrix} - \begin{pmatrix} \frac{1}{s_1} C_1 (R_1 | t_1) \\ \frac{1}{s_2} C_2 (R_2 | t_2) \end{pmatrix} \begin{pmatrix} x_j \\ 1 \end{pmatrix} \right\|^2 \rightarrow \min_{s_i, C_i, R_i, t_i, x_j} \\ \text{s.t. } & x_j^T \begin{pmatrix} 0 \\ 0 \\ 1 \end{pmatrix} = 0 \end{aligned}$$

To solve the optimization problem we use a least square solver from scipy [Jones *et al.*, 2001].

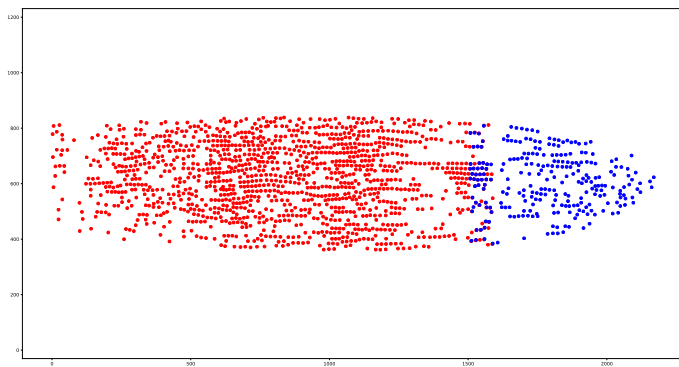
In Figure 4 and Figure 5 we can see examples of projecting the features of two cameras to the laser plane. We can see that the projection seems to work for most particles. But for one in the clipping in Figure 5d the matching is not perfect. The reason is the position in the depth — the particle is not located in the assumed zero-width laser plane.

4.2 Projection to Laser Sheet

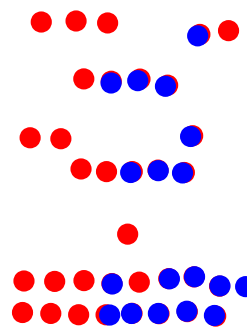
The laser plane can be extended to a laser sheet with a depth described by the parameters $l_l \in \mathbb{R}$, $l \in \mathbb{R}^3$ and $l_u \in \mathbb{R}$:

$$s_i \begin{pmatrix} p_j^{(i)} \\ 1 \end{pmatrix} = P_i \begin{pmatrix} x_j \\ 1 \end{pmatrix} \text{ for all } x_j \in F_{oV} \subset \mathbb{R}^3$$

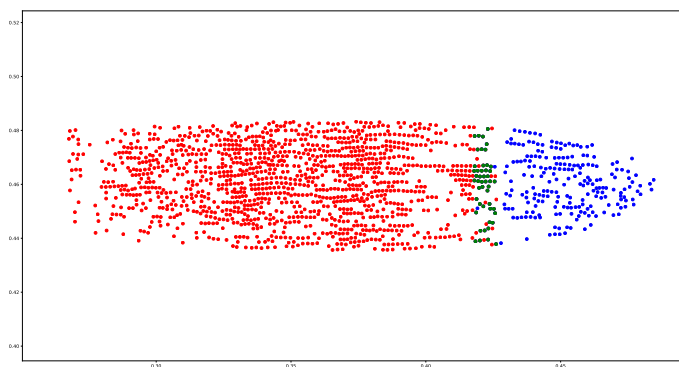
$$\forall x_j \in F_{oV} : l_l \leq l^T x_j \leq l_u$$



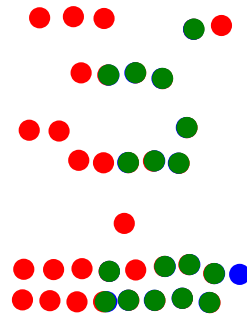
(a) simple combined features



(b) clipping of Figure 4a of the top overlapping region

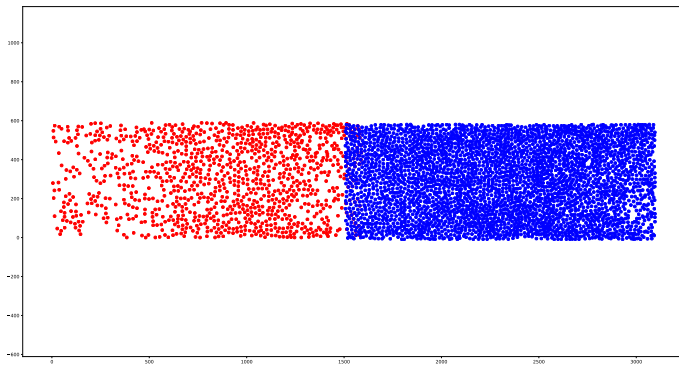


(c) combined features

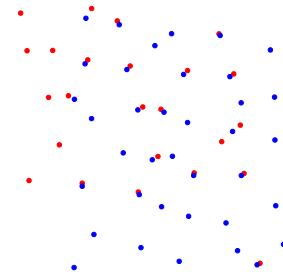


(d) clipping of Figure 4c of the top overlapping region

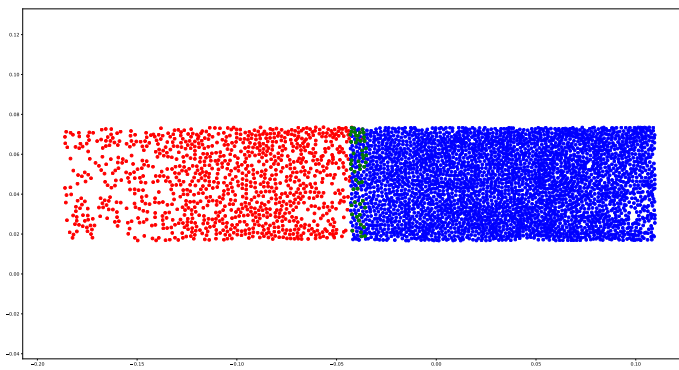
Figure 4: Projection to laser plane: Example with focused laser



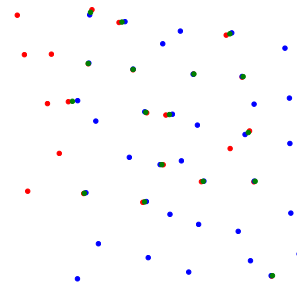
(a) simple combined features



(b) clipping of Figure 5a of the top overlapping region



(c) combined features



(d) clipping of Figure 5c of the top overlapping region

Figure 5: Projection to laser plane: Example with defocused laser

number of cameras	number of corresponding pairs of features	number of scalar unknowns	number of equations
m	n	$nm + 9m + 3n$	$3nm$
2	18	108	108
3	9	81	81
4	8	92	96
5	7	101	105

Table 1: This table shows the number of scalar unknowns and equations (number of residuals of the least square problem) as a function of the number of corresponding pairs of features and the number of cameras. Here it is assumed $f_x = f_y$ and the laser sheet is in the z plane ($-\frac{d}{2} \leq (0, 0, 1) x_j \leq \frac{d}{2}$).

For the example shown in [Figure 4](#) we get 1321 particles in left camera and 259 particles in right camera with 48 corresponding features in the overlapping area. This leads to 274 unknowns and 288 equations.

Again we have to find the best solution (minimized reprojection error) by solving the least square optimization problem:

$$\begin{aligned} \text{obj. func.: } & \sum_{j=1}^n \sum_{i=1}^m \left\| \begin{pmatrix} p_j^{(i)} \\ 1 \end{pmatrix} - \frac{1}{s_j^{(i)}} P_i \begin{pmatrix} x_j \\ 1 \end{pmatrix} \right\|^2 \rightarrow \min_{s_j^{(i)}, P_i, x_j} \\ \text{s.t. } & \forall x_j : \frac{-d}{2} \leq x_j^T \begin{pmatrix} 0 \\ 0 \\ 1 \end{pmatrix} \leq \frac{d}{2} \end{aligned}$$

The number of scalar unknowns and number of residuals of the least square problem is given in [Table 1](#).

In [Figure 6](#) two examples of 3D coordinates are shown, which were determined by solving the optimization problem using a least square solver from [scipy \[Jones et al., 2001\]](#).

5 Conclusion

It seems to be possible to get 3D coordinates ([Figure 6](#)) just from the images of the PK-4 setup [[Pustynnik et al., 2016](#)] in arbitrary units. The resolution approximated in [subsection 2.1](#) can be enhanced by using subpixel resolution as described by [Mohr et al. \[2019\]](#). Using the information from [Pustynnik et al. \[2016\]](#) that 1 px corresponds to about 14 μm allows to calibrate the arbitrary units with physical units.

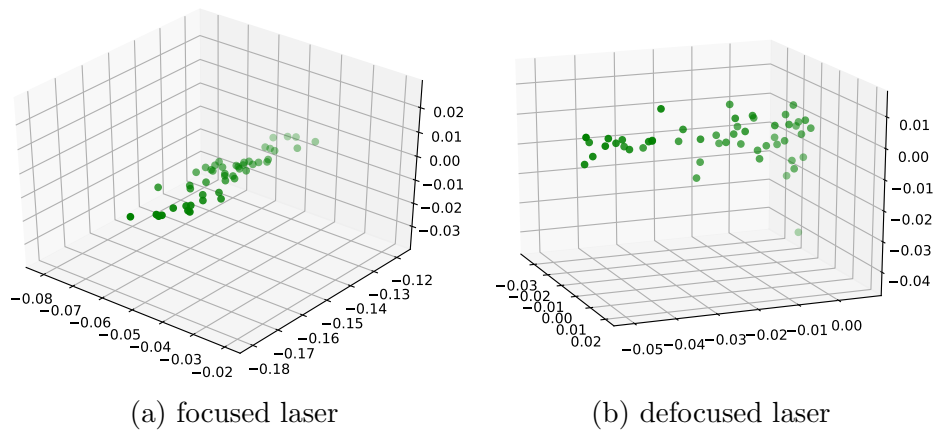


Figure 6: 3D coordinates

References

- G. Bradski. The OpenCV Library. *Dr. Dobb's Journal of Software Tools*, 2000.
- David Claus and Andrew W. Fitzgibbon. A rational function lens distortion model for general cameras. *2005 IEEE Computer Society Conference on Computer Vision and Pattern Recognition (CVPR'05)*, 1:213–219 vol. 1, 2005.
- R. I. Hartley and A. Zisserman. *Multiple View Geometry in Computer Vision*. Cambridge University Press, ISBN: 0521540518, second edition, 2004.
- Michael Himpel, Birger Buttenschön, and Andr'e Melzer. Three-view stereoscopy in dusty plasmas under microgravity: A calibration and reconstruction approach. *Rev. Sci. Instr.*, 82:053706, 2011.
- Eric Jones, Travis Oliphant, Pearu Peterson, et al. SciPy: Open source scientific tools for Python, 2001–. [Online; accessed 2019-02-28].
- Daniel P. Mohr, Christina A. Knapek, Peter Huber, and Erich Zaehringer. Algorithms for particle detection in complex plasmas. *Journal of Imaging*, 5(2), 2019.
- Gregor E. Morfill and Alexei V. Ivlev. Complex plasmas: An interdisciplinary research field. *Rev. Mod. Phys.*, 81:1353, 2009.
- M. Y. Pustyl'nik, M. A. Fink, V. Nosenko, T. Antonova, T. Hagl, H. M. Thomas, A. V. Zobnin, A. M. Lipaev, A. D. Usachev, V. I. Molotkov, O. F.

Petrov, V. E. Fortov, C. Rau, C. Deysenroth, S. Albrecht, M. Kretschmer, M. H. Thoma, G. E. Morfill, R. Seurig, A. Stettner, V. A. Alyamovskaya, A. Orr, E. Kufner, E. G. Lavrenko, G. I. Padalka, E. O. Serova, A. M. Samokutyayev, and S. Christoforetti. Plasmakristall-4: New complex (dusty) plasma laboratory on board the international space station. *Review of Scientific Instruments*, 87(9):093505, 2016.

Mierk Schwabe, Milenko Rubin-Zuzic, Christoph R ath, and Mikhail Pustynnik. Image registration with particles, exemplified with the complex plasma laboratory pk-4 on board the international space station. *Journal of Imaging*, 5(3), 2019.

E. Zaehringer, S. Zhdanov, M. Schwabe, D. P. Mohr, C. A. Knapek, P. Huber, I. Semenov, and H. M. Thomas. Supersonic particle in a low damped complex plasma under microgravity conditions. *AIP Conference Proceedings*, 1925(1):020006, 2018.